Thermal-hydraulic analysis of the DEMO WCLL elementary cell: BZ tubes layout optimization

Francesco Edemetti [a*], Ivan Di Piazza [b], Alessandro Del Nevo [c], Gianfranco Caruso [a]

[a] Department of Astronautical, Electrical and Energy Engineering, Sapienza University of Rome, Roma, Italy
[b] ENEA FSN-PROIN, ENEA CR Brasimone, Camugnano, Italy
[c] ENEA FSN-ING-PAN, ENEA CR Brasimone, Camugnano, Italy

The Water-Cooled Lithium-Lead (WCLL) Breeding Blanket (BB) is a key component in charge of ensuring Tritium production, shield the Vacuum Vessel and remove the heat generated by plasma thermal radiation and nuclear reactions. It relies on PbLi eutectic alloy adopted as breeder and neutron multiplier and refrigerate by subcooled pressurized water. The last function is fulfilled by two independent cooling systems: First Wall (FW) that faces the plasma heat flux and the Breeding Zone (BZ) that removes the deposited power of neutron and photon interaction.

Several layouts of WCLL BB system have been investigated in the last years to identify a configuration that might guarantee EUROFER temperature below the limit (550°C) and suitable thermal-hydraulic performances.

This research activity focuses on the equatorial WCLL elementary cell of the Central Outboard Segment (COB), based on the WCLL BB 2018 design of DEMO 2017 baseline, investigating the cooling performances of the BZ and FW systems and their mutual interaction, verifying the reliability to deliver the coolant at adequate design conditions (i.e. 328°C), evaluating the Eurofer temperature field in order to optimize the BZ Double Wall Tubes (DWTs), extinguishing the hot spot onset into the structures due to the implementation of the IAEA PbLi thermal conductivity as reference.

The goal of the study is to compare three specific different tubes arrangement of the BZ system: the V0.6, that is the reference configuration, the V0.6_A and V0.6_B, identifying and discussing advantages and key issues from the thermal-hydraulics point of view.

The analyses have been carried out using a CFD approach, adopting the commercial ANSYS CFX code, thus a 3D finite volume model of each configuration has been developed. For each WCLL design, several steady-state analyses have been performed, to evaluate the Eurofer temperature field and the thermal-hydraulics performances under different cooling configuration, changing the position of the DWTs. The results show that the FW and BZ system have a mutual interaction. Only the V0.6_B layout can safely remove the high heat loads deposited into the elementary cell, respecting the DEMO requirements. This research activity aims at laying the basis for the finalization of the WCLL BB design.

Keywords: WCLL, CFD, Breeding Blanket, Blanket Engineering.

1. Introduction

The Water-Cooled Lithium Lead (WCLL) Breeding Blanket (BB) is a candidate breeding blanket for DEMO fusion power plant [1]. It must ensure an adequate neutron shielding, tritium breeding self-sufficiency, and energy extraction for electricity production. Lithium Lead (PbLi) is adopted as breeder, neutron multiplier and tritium carrier, Eurofer as structural material, and pressurized water at typical Pressurized Water Reactor (PWR) conditions (15.5 MPa) as First Wall (FW) and Breeding Zone (BZ) coolant. The WCLL BB is designed according to the Single Module Segment (SMS) approach, based on DEMO 2017 baseline, subdivided into 16 sectors, each of them covering a toroidal angular extent of 22.5°. Each of these sectors is composed of three Outboard segments (OB) and two Inboard segments (IB) [2]. To guarantee adequate mechanical properties, the Eurofer must be cooled at a temperature lower than 550°C during the normal operation [3][4].

The thermal-hydraulic studies have the responsibility to evaluate and provide an adequate temperature distribution of the BB verifying the maximum temperature of Eurofer structures, to investigate PbLi heat transfer coefficient in the BZ and to predict the thermal-hydraulic performances of BZ and FW coolant systems. The analyses are focused on the WCLL BB cooling systems, FW and BZ, of the Central Outboard Segment (COB) equatorial elementary cell, that has the highest volumetric power deposition and the lowest Heat Flux (HF) on the plasma-facing surface. Regarding the thermal-hydraulic point of view, the structures temperature field is deeply affected by tubes layout and PbLi thermal conductivity. In literature, there are multiple correlations concerning the thermophysical properties of PbLi, for this reason, it has been considered appropriate to investigate the impact of the conservative thermal conductivity property named IAEA [5] on the model, in order to highlight any hot spot occurrence in the Eurofer structures. A detailed three-dimensional model of the elementary cell is developed, analyzing three different BZ tubes configurations: the V0.6, the V0.6_A, and the

author's email: francesco.edemetti@uniroma1.it

_____

V0.6_B. In particular, the V0.6 presents the reference Double Wall Tubes (DWTs) layout, and the other two geometries have been developed and studied to withstand the presence of the hot spots into the Eurofer.

The main objective of this study is to optimize the DWTs layout of the COB equatorial elementary cell by modifying the layout of the pipes to extinguish the hot spots in the Eurofer structures, ensuring adequate refrigeration. Moreover, the analysis focuses on evaluating the water performance of the BZ and FW systems, in order to verify suitable thermodynamic conditions for the heat exchangers.

2. DEMO WCLL BB

Starting from the main outcomes obtained from WCLL design and analyses [6][7], some optimized designs have been developed.

The WCLL BB 2018 consists of the FW, an external Eurofer structure coated by a Tungsten layer that faces the plasma and water-cooled by square channels with opposite and alternate flow direction, and the BZ, an internal box filled with liquid PbLi alloy water-cooled by the DWTs. The COB equatorial blanket has a toroidal length of 1500 mm and a radial dimension of 1000 mm.

Regarding the BZ system, the PbLi flows through channels defined by Eurofer structural stiffeners and cooled by C-shaped DWTs. The BZ is reinforced with a set of stiffeners to safely withstand the thermo-mechanical loads postulated in normal, off-normal and accidental conditions. Two radial-toroidal stiffeners divide the segment into multiple cells with a poloidal dimension clipped to a height of 135 mm, which is representative of a single elementary cell. Five radial-poloidal stiffeners divide the breeding units in 6 toroidal channels where PbLi flows. A baffle plate, having no structural function, is placed at the half poloidal height, between the two horizontal stiffeners to ensure the circulation of PbLi in radial-poloidal-radial path inside the BZ. A synoptic view of the WCLL 2018 V0.6 elementary cell is shown in Fig. 1.
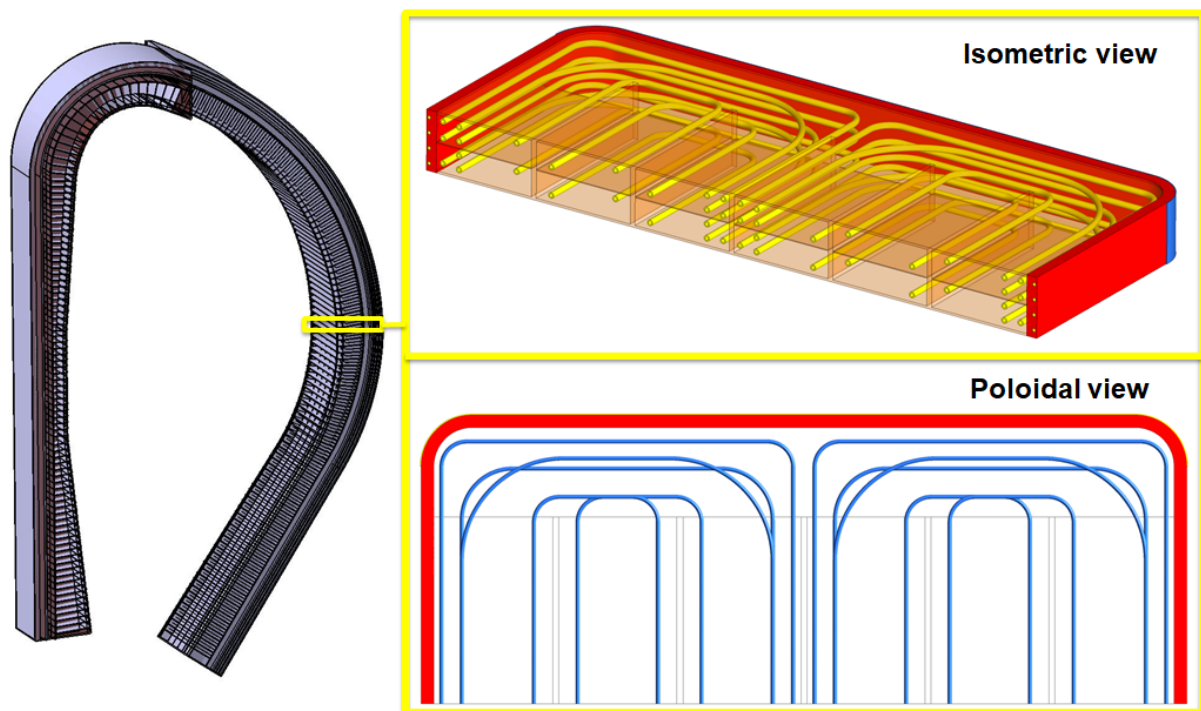

Fig. 1: WCLL 2018 V0.6 COB equatorial elementary cell different view

The BZ cooling system is composed by twenty-two C-shaped DWTs, toroidally symmetric, subdivided in three different arrays, where each array contains both tubes of the two halves [7][8]. Each tube has a hydraulic diameter of 8 mm and an external diameter of 13.5 mm. The tubes arrays are characterized by the geometric position, curvature radius and total length. The first array is composed by six tubes, with a curvature radius of 50 mm, which start from the mid-zone of the toroidal length and radially develop up to the FW, then cover the toroidal length and return in radial direction adjacent the sidewall. The second array concerns eight tubes, having different curvature radius, 100 mm and 200 mm per pair of tubes, poloidally alternated. The two different tubes have a comparable total length; in fact, the tube with the higher curvature radius has a shorter toroidal length, but goes closer to the first array of tubes, and the tube with the lower curvature radius has a longer toroidal length, but is more detached from the FW. The last array has eight tubes, where the tube has the shortest overall length, a curvature radius of 50 mm and cover the central region of the halves with a radial-

_____

toroidal-radial pattern as the previous two arrays. The water enters in the first two arrays in the middle of the cell and exits from the respective outlets located near the side walls by entering the recirculation manifold, after which, it flows into the third array with an opposite flow direction, exiting near the central region [8], as shown in Fig. 2.

Concerning the FW system, it is composed by a U-shaped Eurofer structure 25 mm thick, bent in the radial direction, while the plasma-facing surface is coated by a 2 mm Tungsten armor. The cooling water flows in opposite and alternate flowing direction inside four 7x7 mm channels [9] arranged along the poloidal direction and a uniform pitch.

The BZ and FW systems have the following tasks: to deliver coolant to the Primary Heat Transfer System (PHTS) at the design temperature (i.e. 328°C at 15.5 MPa), to remove the volumetric deposited power into both systems, not exceeding the Eurofer temperature limit of 550°C, and to remove the surface heat load related to the plasma operation that directly impacts the Tungsten armor. The WCLL BZ and FW water-cooling systems operating scheme of the elementary cell is shown in Fig. 2.

_____
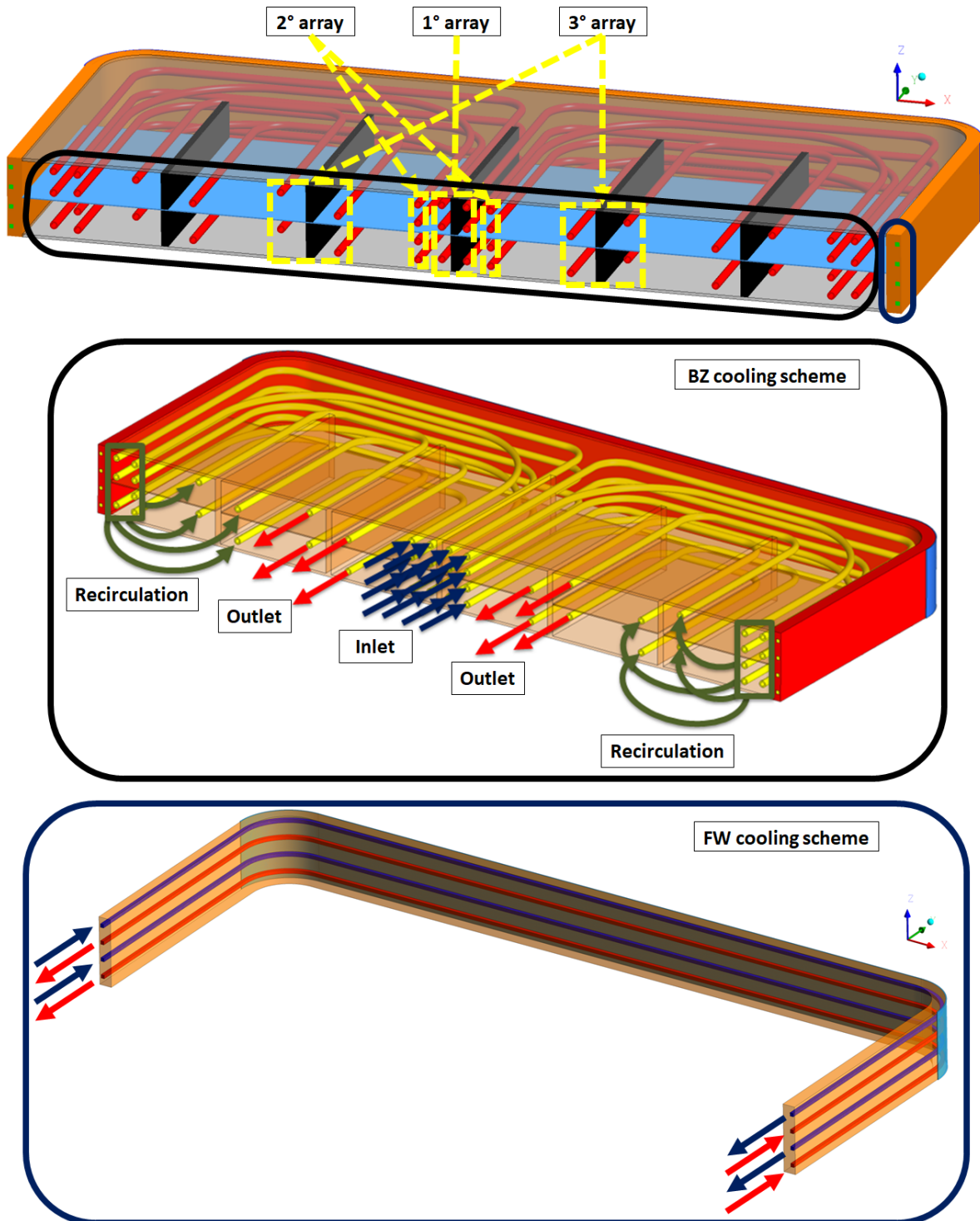
Fig. 2: WCLL BZ and FW water-cooling system operating scheme

2.1. WCLL 2018 V0.6 equatorial elementary cell optimization

As mentioned above, the COB equatorial blanket has a toroidal length of 1500 mm and radial dimension of 1000 mm. In the present analysis, the poloidal dimension of the model is clipped to a height of 135 mm, which is representative of a single elementary cell. Moreover, the model radial dimension is reduced to 567 mm, thus neglecting the section covering the manifold and back supporting structure, where heat loads are foreseen to be negligible.

Three models with different BZ tubes layout are evaluated for steady-state analyses, varying the position of the tubes arrays. The first numerical model is based on the reference layout V0.6, with twenty-two DWTs, divided into three arrays [7] and, concerning the FW cooling system, four channels arranged along the poloidal direction with a uniform pitch [9].

_____

The second and the third configuration, V0.6_A and V0.6_B respectively, have four FW channels but a different BZ tubes layout. The V0.6_A configuration foresees a radial lengthening to the FW of the first array of 5 mm, and a toroidal length reduction of 33 mm of the first and second array to increase the side walls distancing. The V0.6_B changes further the first and second array toroidal length, by reducing 5 mm more from the V0.6_A layout; moreover, the layout of the pipes has been modified enhancing the radial extension of the second array by 5 mm, moving forward to the first array. Concerning the third array, it has been translated by 10 mm from the internal ribs, not modifying the overall tube length. The main changes from the reference V0.6 have been reported in Fig. 3. The main geometrical parameters of the three BZ tubes layout are reported in Table 1.
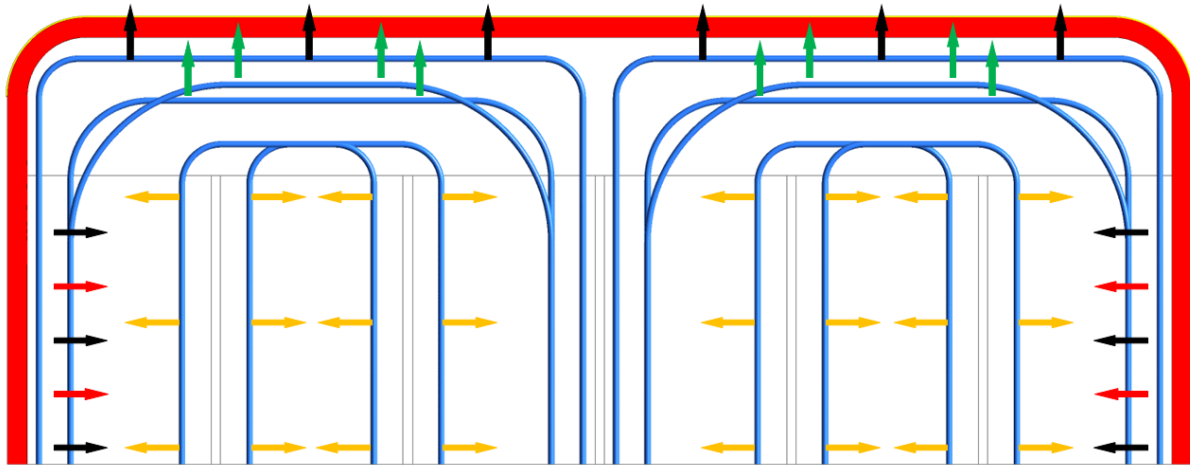

Fig. 3: WCLL V0.6 tubes layout optimization (black arrows – V0.6_A; red, green and yellow arrows – V0.6_B)

Table 1: WCLL different BZ tubes layout and geometrical parameters

Group [-]	Tube [-]	Curve radius [mm]	V0.6 FW dist [mm]	V0.6 Tube Length [mm]	V0.6_A FW dist [mm]	V0.6_A Tube Length [mm]	V0.6_B FW dist [mm]	V0.6_B Tube Length [mm]
1st array	Tube 1	50	20.0	1672.58	15.0	1649.58	15.0	1644.58
	Tube 2	50	20.0	1672.58	15.0	1649.58	15.0	1644.58
	Tube 3	50	20.0	1672.58	15.0	1649.58	15.0	1644.58
2nd array	Tube 4	100	73.0	1443.66	73.0	1410.66	68.0	1415.66
	Tube 5	200	53.0	1397.82	53.0	1364.82	48.0	1369.82
	Tube 6	100	73.0	1443.66	73.0	1410.66	68.0	1415.66
	Tube 7	200	53.0	1397.82	53.0	1364.82	48.0	1369.82
3rd array	Tube 8	50	128.25	1010.08	128.25	1010.08	128.25	1010.08
	Tube 9	50	128.25	1010.08	128.25	1010.08	128.25	1010.08
	Tube 10	50	128.25	1010.08	128.25	1010.08	128.25	1010.08
	Tube 11	50	128.25	1010.08	128.25	1010.08	128.25	1010.08

3. Numerical models

To evaluate the Eurofer temperature field and the thermal-hydraulic performances of the BZ and FW cooling systems, verifying the reliability to deliver the coolant at the design temperature of 328°C to the heat exchangers, and to properly refrigerate the Eurofer structures not exceeding the imposed limit of 550°C, different models of the elementary cell have been set up for the CFD analysis. The 3D finite volume models have been developed according to Sects. 0, using ANSYS CFX v18.2 code, to realistically reproduce the geometry and flow features of WCLL COB equatorial elementary cell and

_____

to obtain a complete and detailed temperature distribution, both in the fluid and the solid domains. In these analyses, fluid domains for BZ and FW water, and solid domains for Eurofer structures, FW Eurofer chase and Tungsten armor have been modelled. Regarding the PbLi domain, it has been modelled as a solid domain, because, it has been evaluated, by simulations with liquid PbLi, that the convective contribution to the heat exchange is almost irrelevant as demonstrated by several CFD simulations considering both diffusive and convective contributions, Refs [7][10][11]. The PbLi reaches, in the case with forced convection and in the absence of buoyancy effects, velocities in the range of v~0.1-0.15 mm/s, resulting in a laminar flow, as the Reynolds number ($Re = \rho \cdot v \cdot L / \mu$) is around 30. Moreover, the Prandtl number ($Pr = \mu \cdot c_p / \lambda$) is close to 0.02, a typical value for liquid metals. This means that the thermal diffusivity, which is related to the rate of heat transfer by conduction, unambiguously dominates prevailing on convection, that can be neglected. Moreover, also the MHD effects strongly reduce the contribution of the convection, suppressing the buoyancy forces, as reported in Refs. [10], [11] where these aspects are discussed. In the present analysis, optimizing the BZ tubes layout to extinguish the Eurofer structures hot spots onset, it has been deemed appropriate to adopt the assumption to model the PbLi as solid domain, since modeling as fluid would not have brought reasonable advantages instead of the computational costs, setting the analyses in a conservativeness condition.

For each configuration, a thermal-hydraulic steady-state analysis has been performed to assess the coolant systems efficiency by removing the total power, as well as sensitivity analyses to optimize the BZ DWTs layout.

3.1. Materials property

The thermophysical properties of water coolant, PbLi, Eurofer and Tungsten have been implemented in the commercial code with a constant value or temperature-dependent function using a polynomial fitting of data [12][13][14]. The properties of Eurofer, Tungsten and PbLi are specified in terms of density, specific heat and thermal conductivity, while water also requires the dynamic viscosity, as summarized in Table 2, Table 3, Table 4 and Table 5, respectively. Regarding the PbLi thermophysical properties, for density and heat capacity the recommended properties of Ref [13] have been adopted, instead, for the thermal conductivity, it has been adopted the IAEA correlation [5] to perform conservative analyses, due to a mean percentage difference of 32% from the Mogahed recommended correlation [15].

Table 2: Tungsten thermo-physical properties (T in K) [12]

Value	Unit
$\rho = 19300$	kg/m³
$c_p = 145$	J/(kg K)
$\lambda = 125$	W/(m K)

Table 3: Eurofer thermo-physical properties (T in K) [12]

Equation	Unit
$\rho = 7874.3 - 0.361 \cdot T$	kg/m³
$c_p = -438.83 + 4.9838 \cdot T - 8.7371 \cdot 10^{-3} \cdot T^2 + 5.3333 \cdot 10^{-6} \cdot T^3$	J/(kg K)
$\lambda = 60.915 - 9.081 \cdot 10^{-2} \cdot T + 6.5 \cdot 10^{-5} \cdot T^2$	W/(m K)

Table 4: PbLi thermo-physical properties (T in K) [13]

Equation	Unit
$\rho = 10520.35 - 1.19051 \cdot T[K]$	kg/m³
$c_p = (0.195 - 9.116 \cdot 10^{-6} \cdot T[K]) \cdot 10^3$	J/(kg K)
[5] $\lambda = 11.9 + 1.96 \cdot 10^{-2} \cdot (T[°C] - 235)$	W/(m K)

Table 5: Water thermo-physical properties (T in K) [14]

Equation	Unit

$\rho = -1.4226 \cdot 10^{-2} \cdot T^2 + 14.122 \cdot T - 2693$	kg/m³
$c_p = 9.8485 \cdot 10^{-3} \cdot T^3 - 16.39861 \cdot T^2 + 9118.681 \cdot T - 1.6882247 \cdot 10^6$	J/(kg K)
$\lambda = -1.2024 \cdot 10^{-5} \cdot T^2 + 1.1846 \cdot 10^{-2} \cdot T - 2.2804$	W/(m K)
$\mu_d = (-8.095238 \cdot 10^{-4} \cdot T^2 + 0.5722429 \cdot T + 29.67213) \cdot 10^{-6}$	kg/(m s)

3.2. DEMO WCLL BB thermal loads

The thermal loads in the WCLL BB are mainly caused by two sources: the neutron flux generated by the fusion reaction and thermal radiation between plasma and facing materials and they can be assumed constant during these analyses. These phenomena can be represented with a volumetric power density into materials and a heat flux applied to the Tungsten armor.

According to Ref. [16], the elementary cell under analysis has its own power curves, that radially decrease moving from the Tungsten to the backplate. The Eurofer power curve reaches its maximum in the Tungsten layer, and the PbLi curve has its maximum at the FW-BZ interface, both radially decrease. To realistically reproduce the radial power deposition trend into PbLi and solid structures, multiple curves have been created to obtain an appropriate power deposition trend into the cell. Two different set of equations have been implemented in the models, which represent the Eurofer and the PbLi power deposition trend, shown in Fig. 4. The heat flux, composed of charged particles and thermal radiation, impacts the whole Tungsten armor that faces the plasma. According to [17] and [18], a maximum nominal value of 0.32 MW m⁻² is imposed onto the straight armor surface. Concerning the elbows, a decreasing linear trend equation with the radial direction is implemented, this to take into account the decrease in the normal component of the heat flux, due to the variation of the incidence angle, $q''_{SW} = \left[1 - \frac{(y_0 - y)}{y_{tot}} \right] \cdot q''_{max}$.
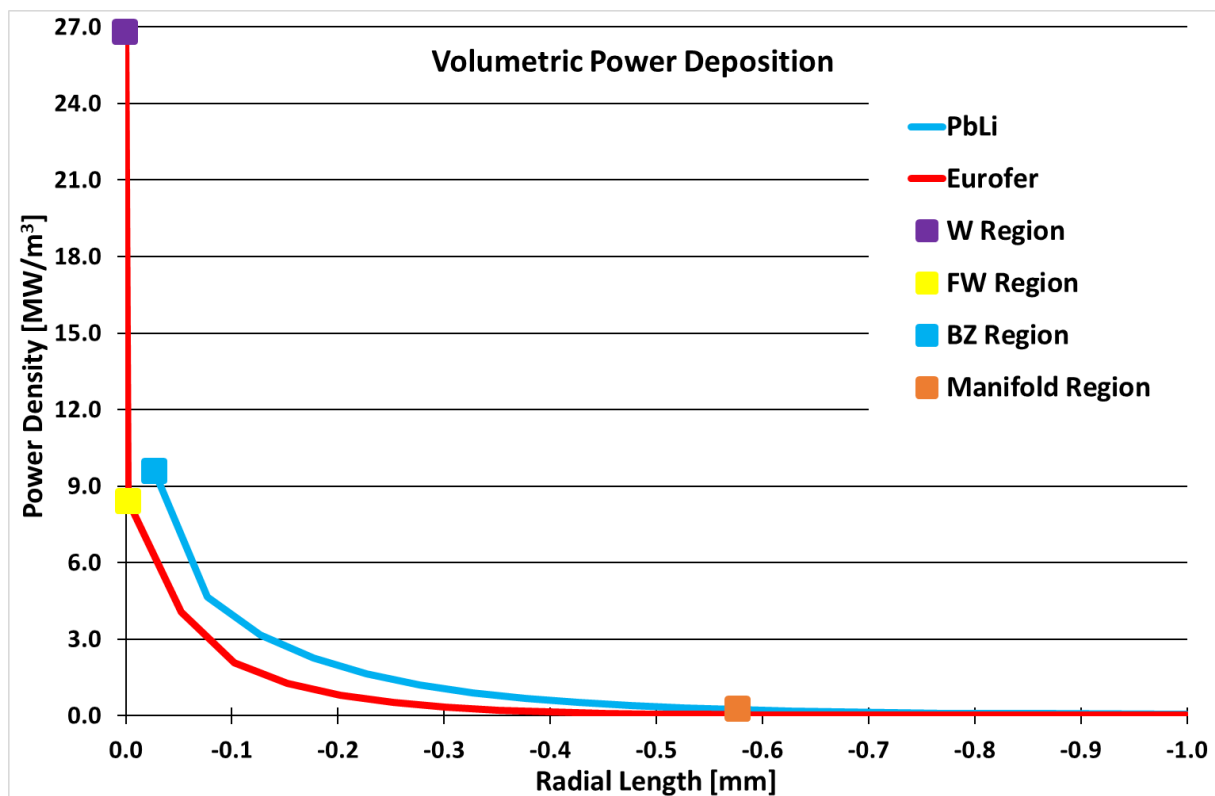

Fig. 4: WCLL BB COB equatorial cell radial volumetric power deposition

3.3. Boundary conditions and solver setting

For each steady-state analyses, the reference water thermodynamic cycle is assumed as in the WCLL BB 2017 design [12][19][20]. The cycle, still based on PWR conditions, foresees water coolant entering at 295°C and exiting at 328°C, at 15.5 MPa. The imposed total water mass flow rate remains constant in each run; it has been evaluated with the enthalpy balance using RELAP5/Mod3.3 water properties [14], to obtain in all the analyses an outlet water temperature of 328°C.

_____

The BZ cooling system has an imposed water mass flow rate of 0.85491 kg/s, firstly equally divided by the fourteen tubes of the first and second arrays and then equally divided by the eight tubes of the third array (Fig. 5 a). The FW water mass flow rate is 0.63189 kg/s, equally distributed on the four channels (Fig. 5 b). The FW water inlet temperature is equal to 295°C, instead, since BZ has recirculation, the water enters in the cooling system at 295°C in the first and second arrays, and then re-enters into the tubes of the third array for the second passage at the average outlet temperature obtained from the first passage, thus simulating a perfect mixing.

The other boundary conditions adopted for all the models are:

- Periodic boundary conditions on the upper and lower surfaces of upper and lower stiffening plates, FW and Tungsten layer, in poloidal direction, to simulate the presence of adjacent elementary cell;
- Adiabatic condition to back walls of FW, stiffeners, Tungsten layer and FW side walls;
- Mass flow rate and static pressure imposed in the fluid domain at inlet and outlet sections, respectively;
- No-slip condition at the interface between coolant and the circuit steel walls.

The average Reynolds number is around 210000 in the BZ system and 275000 in the FW system, resulting in turbulent flow for both systems and all models. The two-equations k-ω Shear Stress Transport (SST) model has been selected as an appropriate method to simulate the turbulence effects because it is able to solve the viscous sublayer explicitly with $y^+ \le 1$ without losing accuracy in the free stream of the channels, as reported in Ref. [21]. Moreover, it has been applied to a large variety of similar turbulent flows (Refs. [7], [9], [12] and [20]). In addition, the model represents an acceptable compromise between accuracy and robustness [22].

A detailed set of the imposed boundary conditions is reported in Fig. 5.

a) BZ Water inlet and outlet BCs

b) FW Water inlet and outlet BCs

c) Different domain BCs
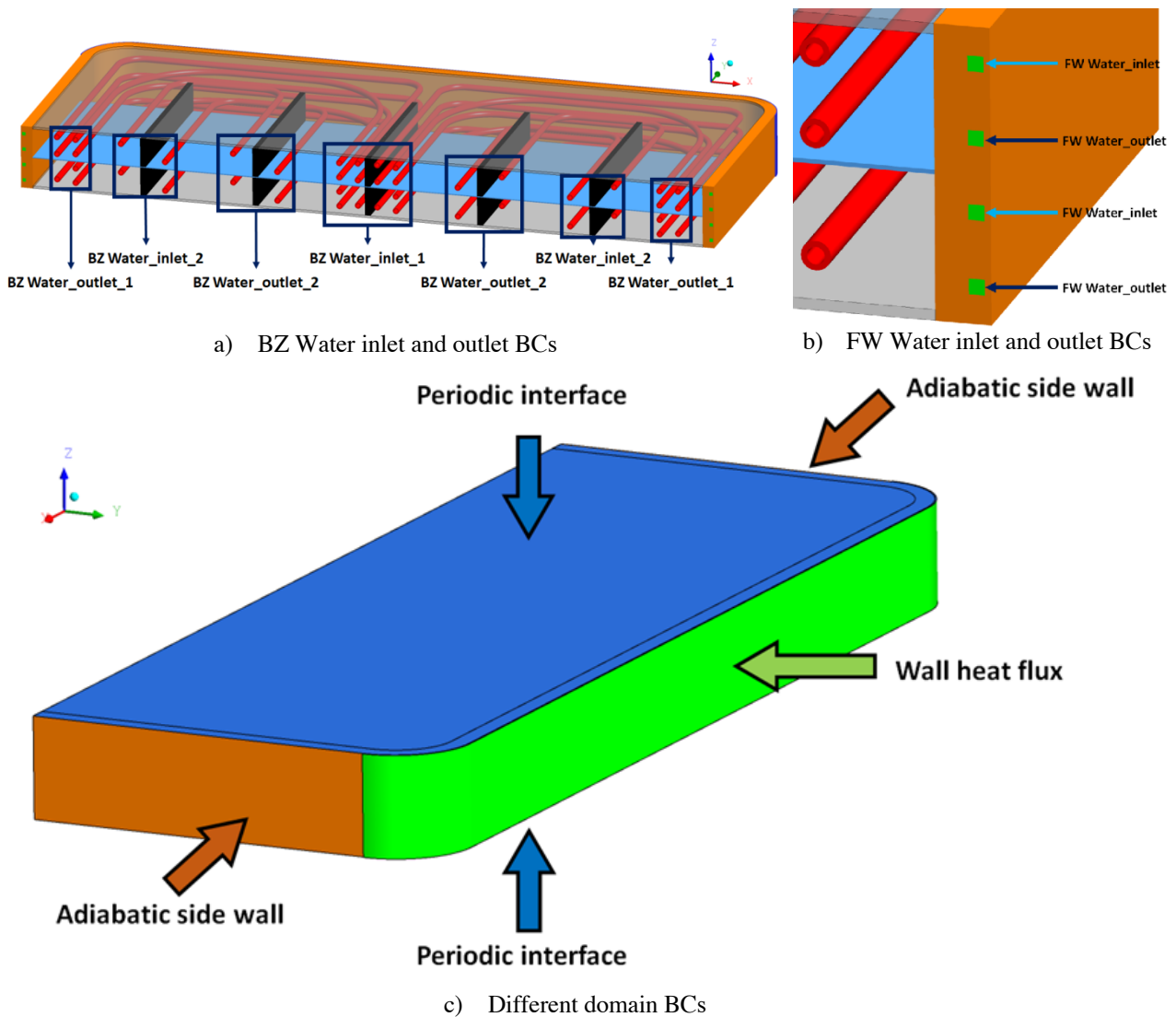
Fig. 5: WCLL COB equatorial elementary cell boundary conditions

_____

3.4. Mesh independence analysis

For the models, a mesh independence analysis has been performed, allowing accurate results and reasonable calculation time, using meshes with different degree of detail. All the geometrical models are developed as a single part, to simulate the heat transfer between the multiple components, solids and fluid using a conformal mesh. Hexahedral and tetrahedral elements were adopted in the models, considering the geometrical features of the domains, many and different local controls are inserted to define the complex geometry of the cell properly. For this purpose, different code tools were exploited, such as sizing control, sweep method, mapped face, and the inflation control near the solid walls for the resolution of the viscous sub-layer ($y^+=1$) of the water, based on a maximum velocity of 7 m/s.

The analysis was conducted to establish the independence of results from the grid and to optimize the number of elements in the model. The simulations have been reported and proved in Ref. [12] for a COB equatorial elementary cell with the same geometry and a similar DWTs distribution. A mesh detail is shown in Fig. 6, and the mesh statistics of each numerical model are reported in Table 6.


a) FW and BZ water domain   b) PbLi and stiffeners domain
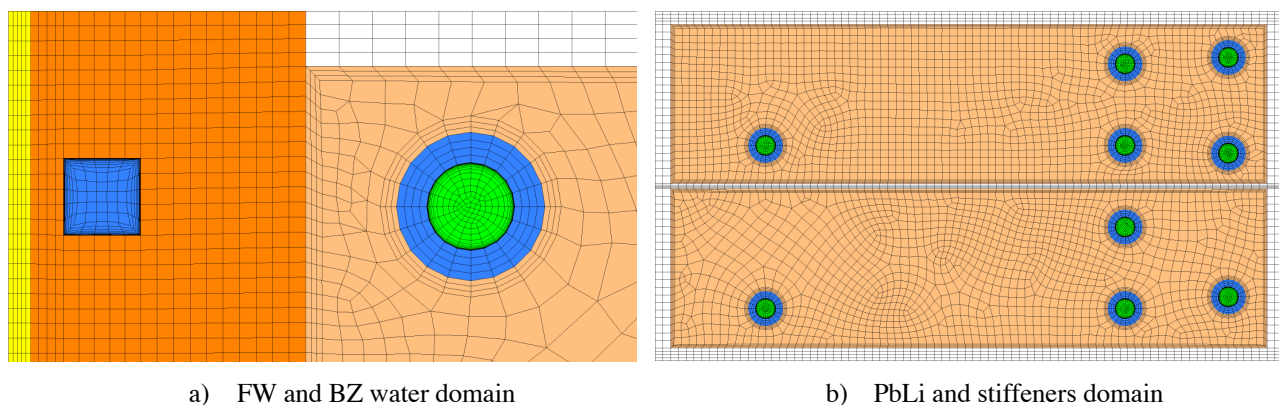
Fig. 6: WCLL COB equatorial elementary cell V0.6 mesh detail

Table 6: Numerical models mesh statistics

Model	N° Nodes	N° Elements	Average Orthogonal Qual	Average Skewness
V0.6	14.65M	19.76M	0.8420	0.1805
V0.6_A	15.97M	19.38M	0.8519	0.1799
V0.6_B	15.02M	19.41M	0.8516	0.1791

4. Results and discussion

The results of the three runs performed are discussed below. The models differ by the position of the BZ double-wall tubes. The analyses have been performed in steady-state conditions to optimize the layout of the tubes, obtaining a detailed temperature map of the Eurofer structures and evaluating the water thermal-hydraulic conditions.

The relevant parameters of the steady-state runs are reported in Table 7, where, it is clearly shown that the Eurofer temperature exceeds the maximum allowable value of 550°C in the V0.6 and V0.6_A configurations in all the plates, upper, lower and baffle. Concerning the V0.6_B layout, the Eurofer maximum temperature is below the limit for both plates, upper and lower; conversely, the baffle plate returns a maximum temperature of 552.1°C. The adopted recirculation manifold of the BZ water cooling system guarantees maximum water temperatures below the saturation temperature for the second and third arrays in all the cases, and slightly exceeds it in the first array. The BZ recirculation also ensures higher velocities, enhancing the cooling performances in all the arrays, obtaining comparable velocities in the first and second array and almost doubled in the third. The BZ pressure drops due to the recirculation are, however, reduced if compared with the FW cooling system, which turns out to be 5 times higher. All the three configurations provide as water average outlet temperature, for both BZ and FW cooling systems, of 328°C. The obtained results are hereafter discussed, divided by models.

_____

Table 7: Steady-state analyses: main output parameters

Parameters	Configuration			Unit
	V0.6	V0.6_A	V0.6_B	
Tungsten T max	488.8	485.5	485.5	°C
FW T max	513.9	505.0	504.8	°C
Upper Plate T max	557.5	557.4	543.7	°C
Lower Plate T max	557.7	557.6	543.9	°C
Baffle T max	566.2	566.2	552.1	°C
PbLi T max	600.7	587.6	584.7	°C
FW Water_outlet T ave	328.2	328.3	328.4	°C
FW Water T max	363.0	363.1	363.2	°C
BZ Water_outlet_2 T ave	328.1	328.0	327.9	°C
BZ Water 1st array T max	352.7	354.7	353.3	°C
BZ Water 2nd array T max	342.3	338.2	337.8	°C
BZ Water 3rd array T max	341.2	341.2	341.9	°C
FW Water_outlet v ave	4.923	4.924	4.925	m/s
FW Water v max	5.817	5.819	5.820	m/s
BZ Water_oulet_2 v ave	3.294	3.293	3.292	m/s
BZ Water 1st array v max	2.167	2.176	2.170	m/s
BZ Water 2nd array v max	2.111	2.103	2.104	m/s
BZ Water 3rd array v max	3.975	3.965	3.965	m/s
FW Water_inlet P drop	41.526	41.107	41.115	kPa
BZ Water_inlet_1 P drop	4.084	4.009	4.008	kPa
BZ Water_inlet_2 P drop	7.918	7.896	7.899	kPa

4.1. V0.6 Configuration results

Regarding the reference layout V0.6, as reported, the Eurofer maximum temperature exceeds the imposed limit of 550°C. Given the results obtained in Ref. [7], where the two thermal conductivity of the PbLi Mogahed [15] and IAEA [5] are compared and where the latter reaches a Eurofer temperature field of the plates about 50 degrees higher, it is clear that this analysis has a comparable Eurofer thermal field as in Ref. [7], confirming that the present analysis has been performed with conservative BCs allowing the BZ tubes optimization to extinguish the hot-spots onset into the Eurofer structures.

Regarding the structural materials, the V0.6 returns a symmetrical temperature field in toroidal direction and concerning the FW system also in the poloidal length, due to the opposite and alternate flow of the water and the constant poloidal pitch of the channels (Fig. 7 a). The configuration results below the required limit of 1300°C for the Tungsten layer, and regarding the Eurofer limit, only the FW chase satisfy the requirement reaching a maximum temperature of 513.9°C. In Fig. 7 (b), a radial-poloidal cut at the middle of the FW toroidal length shows that the internal part of the FW (FW-BZ interface) is warmer than the external region (FW-Tungsten interface). Comparing the FW system with that described in [9], Fig. 7 (b) shows a different temperature field. In the present analysis, (FW system with 4 water channels) a maximum temperature 50 degrees higher than the value shown in [9] is reached; moreover, the imposed water mass flow rate, necessary to guarantees 328°C at the FW outlet, is increased by 13%; this means that the FW passively removes some thermal power from the BZ system, as suggested in [9]. The two plates slightly exceed the limit, as opposed to the baffle which exceeds it by 16.2 degrees. In order to evaluate the temperature distribution into the plates, the Eurofer lower plate temperature field has been reported in Fig. 8, where the grey regions exceed the maximum allowable temperature of 550°C. As shown, the FW chase is below the requirement, and two hot spot regions in the plate are shown. The first

one is located in the frontal part near the BZ-FW interface, caused by the curvature of the first tube array and a FW detachment of 20 mm; the second hot region is at the end of the baffle plate, in the middle of the sub-unit of the cell, where the tubes of the third array are 20 mm distanced from the ribs structures and their influence on the central region is weak, thus causing the onset of a hot spot. Moreover, the side walls region is well cooled and stands around 350°C.


a) FW Eurofer chase temperature field

b) FW system radial poloidal view at half toroidal length
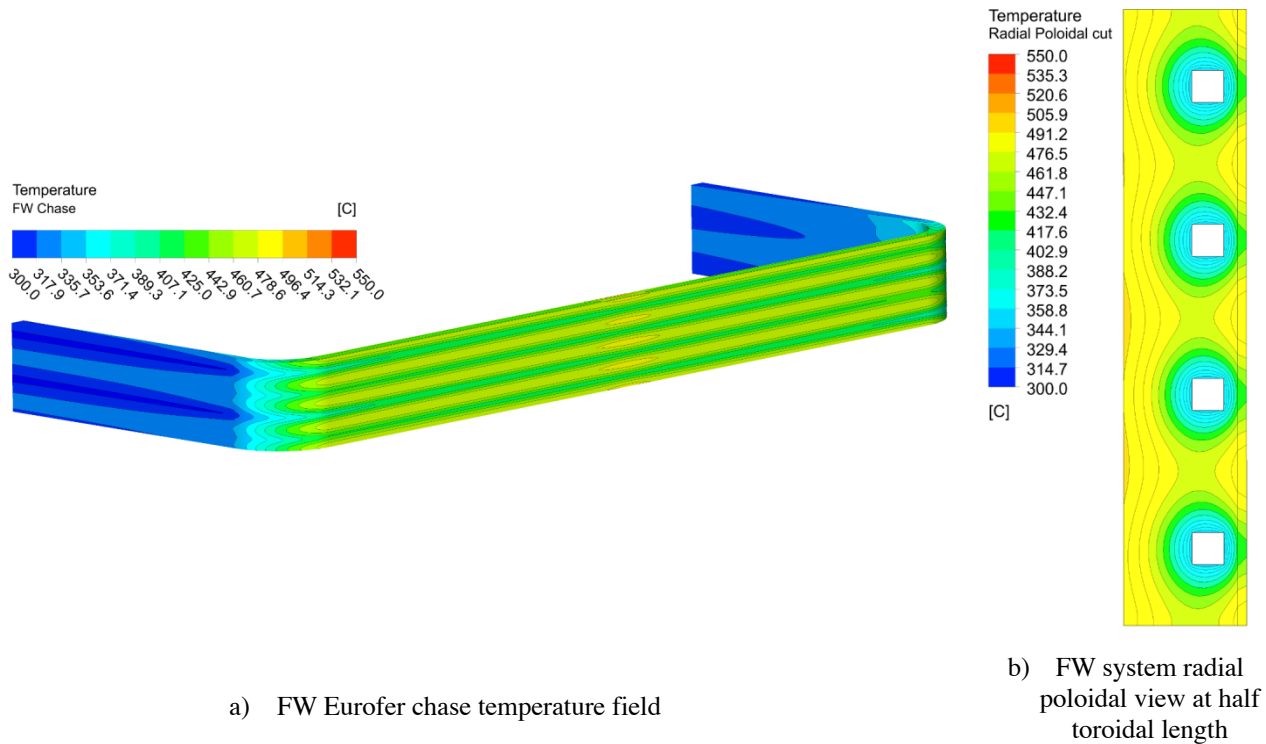
Fig. 7: V0.6 elementary cell FW chase temperature distribution
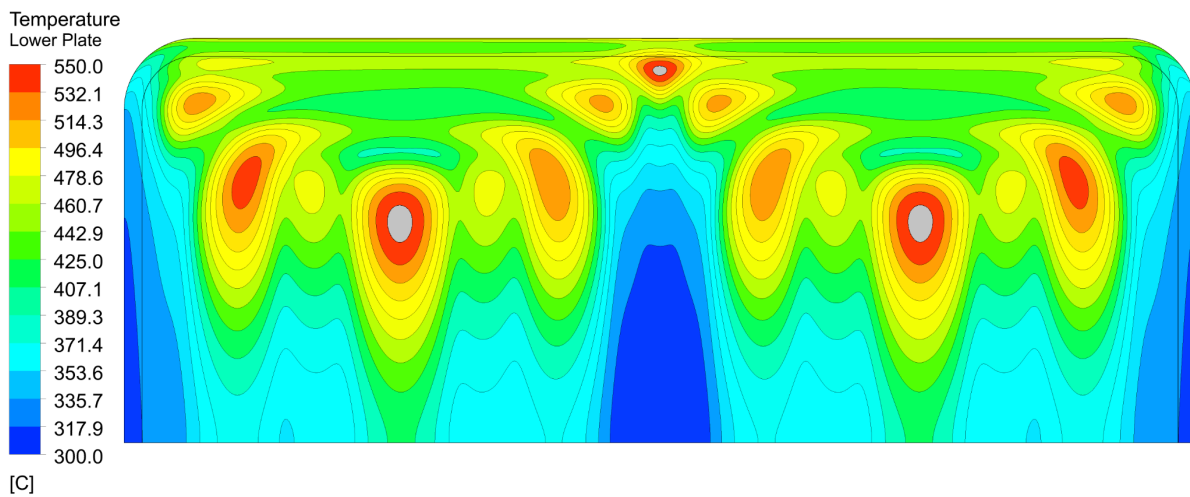
Fig. 8: V0.6 elementary cell lower plate temperature distribution

Considering the FW and BZ water coolant systems, as expected, the water outlet temperatures, averaged on the mass flow rate and the overall outlet tube sections, are very similar: 328.2°C and 328.1°C respectively. Analyzing the maximum water temperature, the first array and in the FW channels exceed the saturation value (344.8°C at 15.5 Mpa) in both systems, which should result in a local boiling, but in the CFX numerical model the phase change is not considered. The possibility of thermal crisis occurrence has been then evaluated. For horizontal tubes and high flow rates, according to Ref. [23], the Critical Heat Flux (CHF) can be predicted using the correlation $q''_{CHF,Hor} = k * q''_{CHF,Ver}$, where the parameter k varies with the Froude number $Fr = {G^2}/{(\rho_L^2 g D)}$, where G is the total mass flux (kg/m² s), ρ_L is the density

_____

of the saturated liquid at 15.5 MPa (kg/m³), g is the gravity acceleration (m/s²) and D corresponds to the diameter of the tube (m); q"$_{CHF,Ver}$ is the correlation for the vertical channels subjected to the same heat flux. The value of k is calculated in term of Fr number as $k = 0.725 * Fr^{0.082} \leq 1$. Thus, if k is greater than 1, k=1 is adopted and also k=1 at Fr number greater than 50. Regarding the two systems, Fr = 53.3 and 428.5, are obtained, thus is imposed k=1 for both. The Tong's correlation [24] has been adopted to evaluate the q"$_{CHF,Ver}$, obtaining q"$_{CHF,Hor}$ = 2.76 MW/m² and 3.42 MW/m² for the first array and the FW channels respectively. The maximum heat flux that affects the first array and the FW channels is 0.701 MW/m² and 1.096 MW/m². Therefore, no thermal crisis within the first array and the FW channels occurs, but it is likely that limited areas of the channel wall can exist where subcooled nucleate boiling is the dominant heat transfer regime. The analysis of the stand-alone FW system (Ref. [9]) has demonstrated that the calculated CHF is lower, passing from 3.15 to 3.42 MW/m² of the present analysis, enhancing the margin from the thermal crisis. Moreover, the obtained maximum heat flux slightly differs from the stand-alone system, reducing its value by 1%.

Regarding the PbLi, in Fig. 9, two different radial poloidal cuts are presented. The Fig. 9 (a), in correspondence with the frontal hot spot, shows how the curvature radius of the first tube array causes a hot column region above 550°C which impacts the two Eurofer plates. Moreover, it shows how the FW system contributes to cool down that region, limiting the hot spot radial extent. In the figure, it is also reported how the central rib is refrigerated by the DWTs inlet, returning a temperature distribution more than 200 degrees below the imposed limit. The Fig. 9 (b), located at the baffle plate hot spot, shows a wider hot spot column, where the third tubes array has no influence on the Eurofer structures.
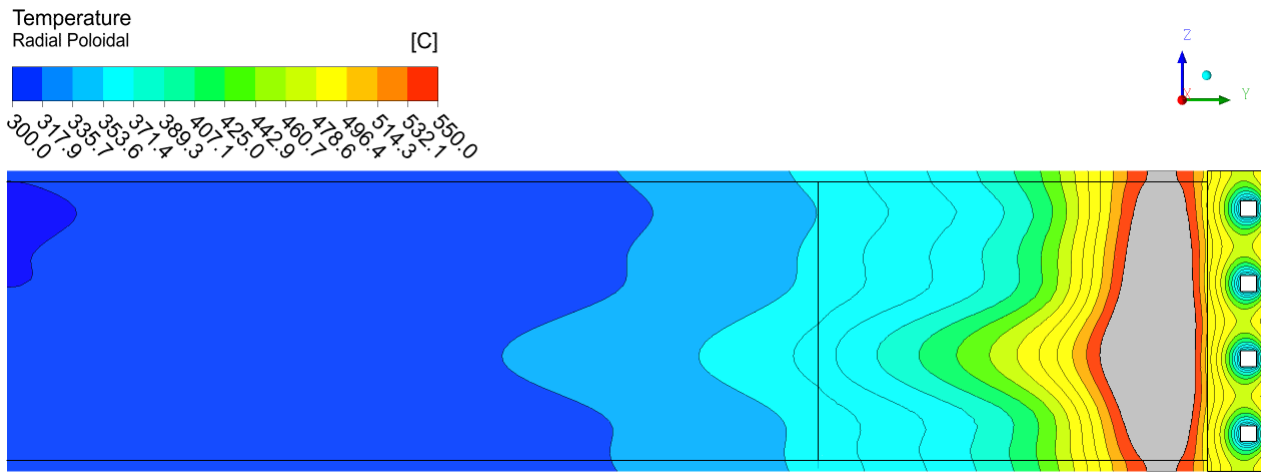
a) Radial poloidal view at the frontal hot spot
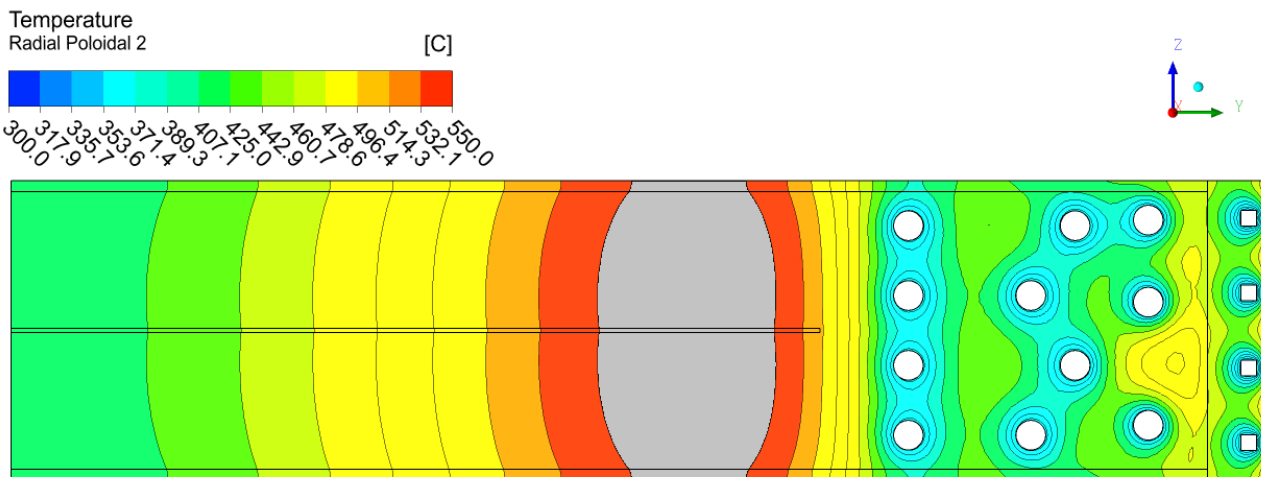
b) Radial poloidal view at the baffle plate hot spot

Fig. 9: V0.6 elementary cell radial poloidal plane temperature distribution

4.2. V0.6_A Configuration results

_____

Regarding the V0.6_A optimization, which provides the reduction of the first tubes array detachment from the FW and the reduction of the toroidal length of the first and second arrays, it returns an improved, but still not entirely satisfactory temperature field. The Eurofer structures of the elementary cell V0.6_A, as in the previous case, have a symmetrical temperature field. The decrease of the distance between the first tubes array and the FW chase, achieves the refrigeration of the frontal hot spot, obtaining a temperature lower than the fixed limit of 550°C, as shown in Fig. 10. With the reduction of the toroidal tube length, the hot spot at the baffle plate is still present, as in the previous V0.6 case. As shown from the temperature field of the lower plate, it is clear that reducing the tubes toroidal length, the temperature field in the upper corner near the side walls bent increases, albeit within the limit.
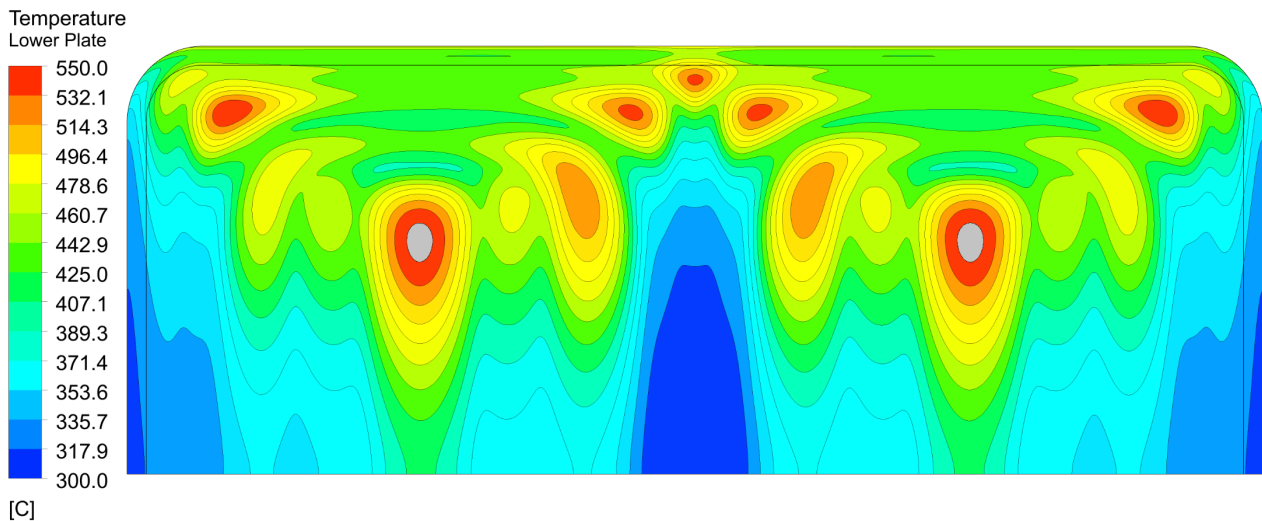
Fig. 10: V0.6_A elementary cell lower plate temperature distribution

The FW system benefits from the distance reduction between the first tubes array and FW chase, decreasing its maximum temperature by about 9 degrees. The maximum temperature of Tungsten is not affected by the variation of the BZ tubes: a slight decrease of only 2 degrees has been calculated. The temperature distribution of the two domains of the FW system is shown in Fig. 11. The Fig. 11 (b) shows how the FW internal part is affected by the first array movement, the isotherm of the internal part are flatten towards the water channels running into the concentric isotherm generated by the water channels. A different trend has been obtained in Ref. [9], where the isothermal lines, obtained from the water channels, show a symmetrical airfoil trend starting from the Tungsten up to the internal part of the FW. A greater balance between the passive heat supplied by the BZ system and that generated in the FW is noted.
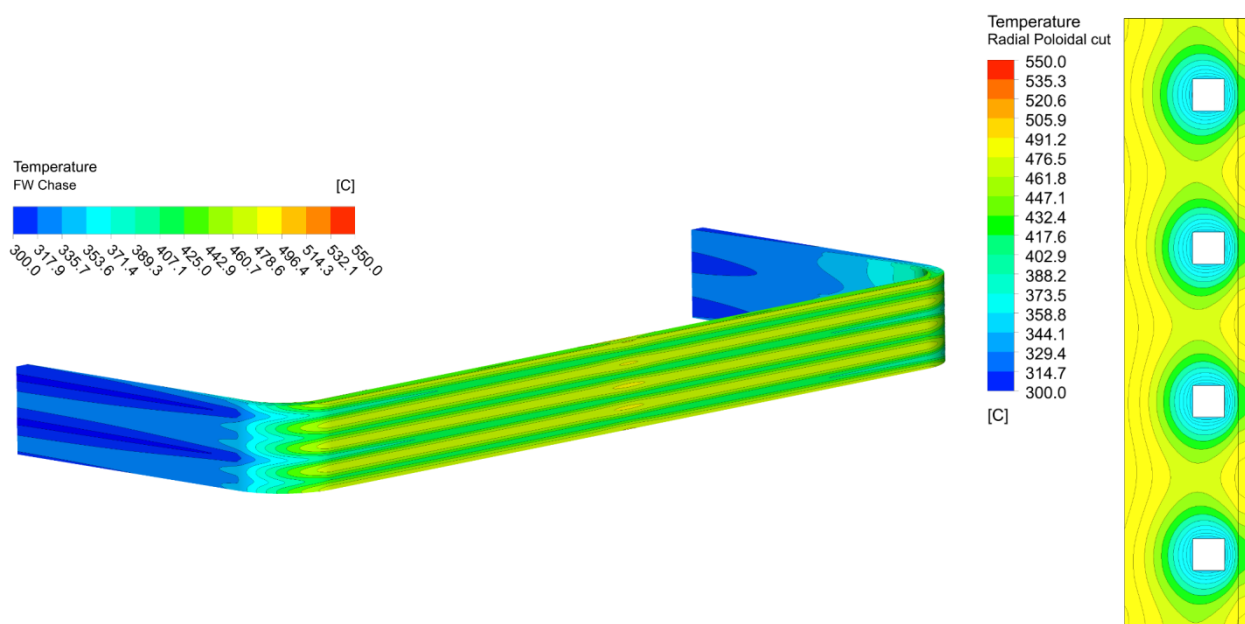
_____

a) FW Eurofer chase temperature field

b) FW system radial poloidal view at half toroidal length

Fig. 11: V0.6_A elementary cell FW system temperature distribution

As expected, the average outlet temperature in both FW and BZ cooling systems is 328.3 and 328°C, respectively. Concerning the maximum water temperature, it reaches 363.1 in the FW channel and 354.7°C in the first BZ array. The CHF has been evaluated with the same correlation used in the V0.6 analysis, in terms of k and Fr number. Thus, for both FW channel and BZ tube k = 1, due to Fr = 428.5 and 53.3, respectively. The CHF is evaluated, like in the previous cases, obtaining 3.42 for the FW and 2.76 MW/m² for the BZ, values to be compared with actual ones 2.9 and 4.0 times lower in the two systems, respectively. Therefore, the V0.6_A has higher margin to avoid the thermal crisis.

The radial-poloidal temperature profile is shown in Fig. 12. The (a) reports that the reduction of the FW detachment of the tubes from the FW has reduced the frontal hot spot region, concentrating entirely within the PbLi and greatly reducing its area, but in (b) is clear that this BZ tubes layout had no effect on the baffle plate region, even enhancing the side walls detachment.
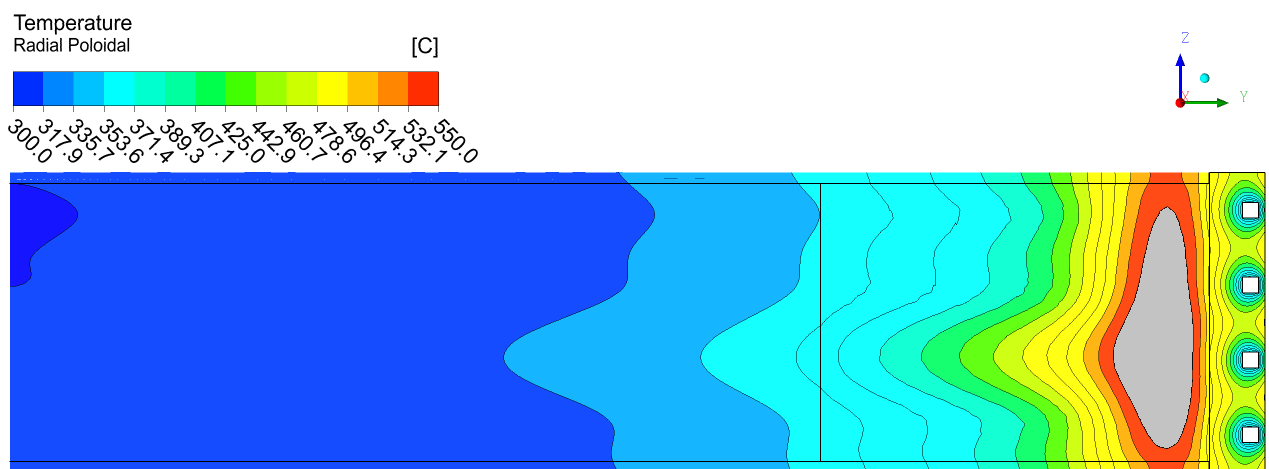
a) Radial poloidal view at the frontal hot spot
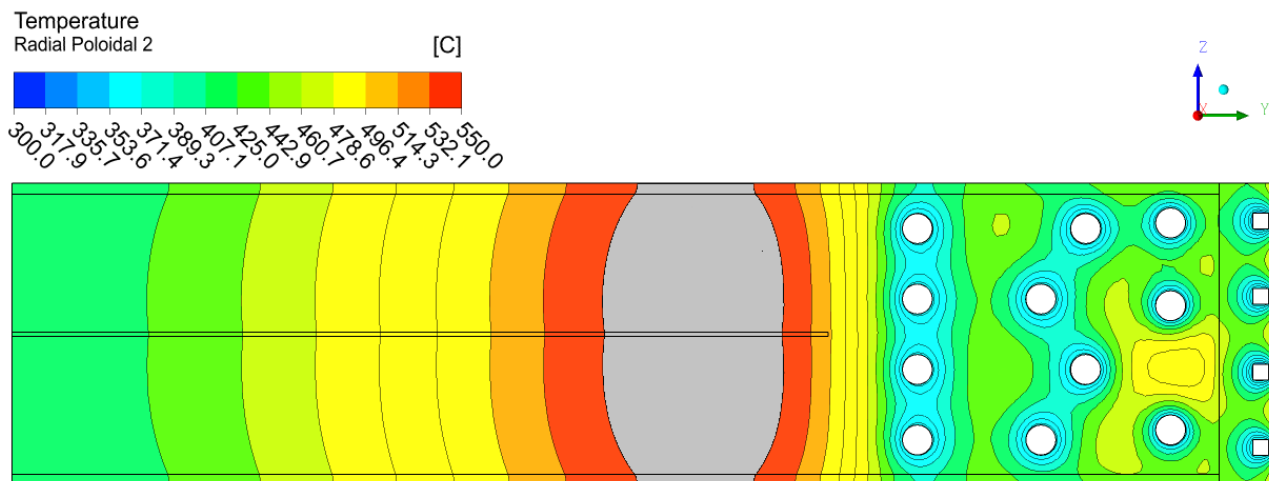
b) Radial poloidal view at the baffle plate hot spot

Fig. 12: V0.6_A elementary cell radial poloidal plane temperature distribution

4.3. V0.6_B Configuration results

The last analyzed BZ configuration V0.6_B, with a further toroidal length reduction of the first and second arrays, an increased radial path for the second tubes array and a rigid detachment from the ribs of the third array, as discussed in

_____

Sect. 2.1, returns a Eurofer temperature field below the imposed limit for the FW chase, upper and lower plates domains, as reported in Table 7; only the baffle plate exceeds by 2 degrees the temperature limit. The V0.6_B tubes layout extinguish all the hot spots presented into the plates, ensuring a maximum temperature, below the limit of 550°C, of about 7 degrees for both plates. The plates temperature field is toroidally symmetric, as in the previous analyses. The lower plate is shown in Fig. 13, where, the baffle plate hot spot region is not present; this implies that this BZ layout affects the baffle region of the previous version. Moreover, the hot spots in the upper corners near the sidewalls have reduced their area due to the radial length extensions of the second array that contributes to refrigerate those regions.
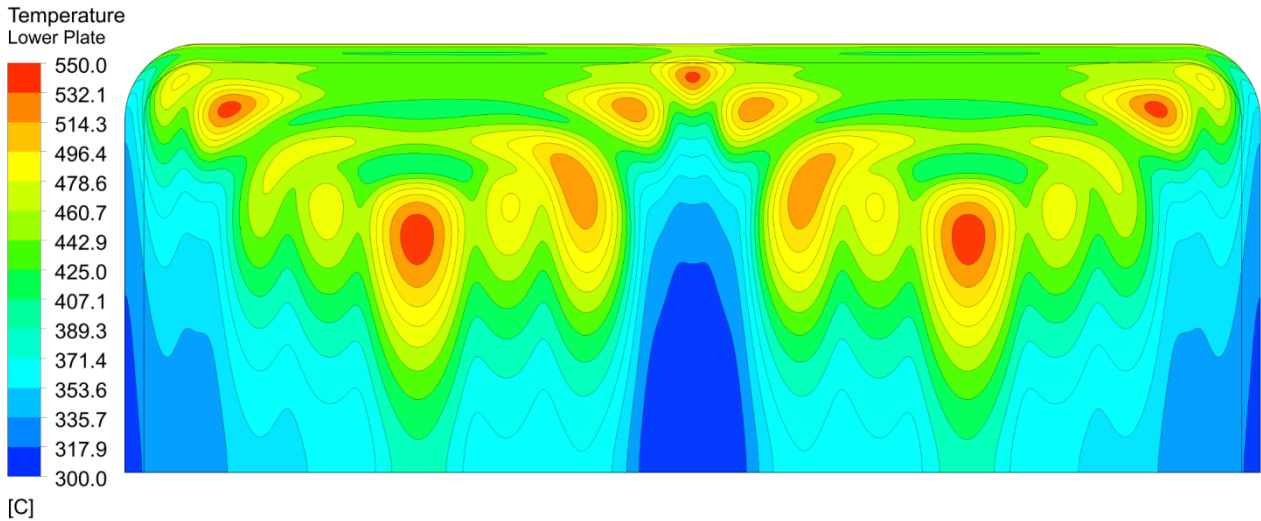

Fig. 13: V0.6_B elementary cell lower plate temperature distribution

Regarding the FW system, the solid domain of FW chase and Tungsten present a maximum temperature of 504.8 and 485.5 °C, respectively. The maximum temperature value of the FW chase is higher than in the Tungsten layer, because of the BZ thermal interaction with the FW by passive heat exchange, heating the inside part of the latter (Fig. 14 a). Regarding the radial-poloidal temperature distribution, shown in Fig. 14 b, no significant variation compared with the V0.6_A has been evidenced.
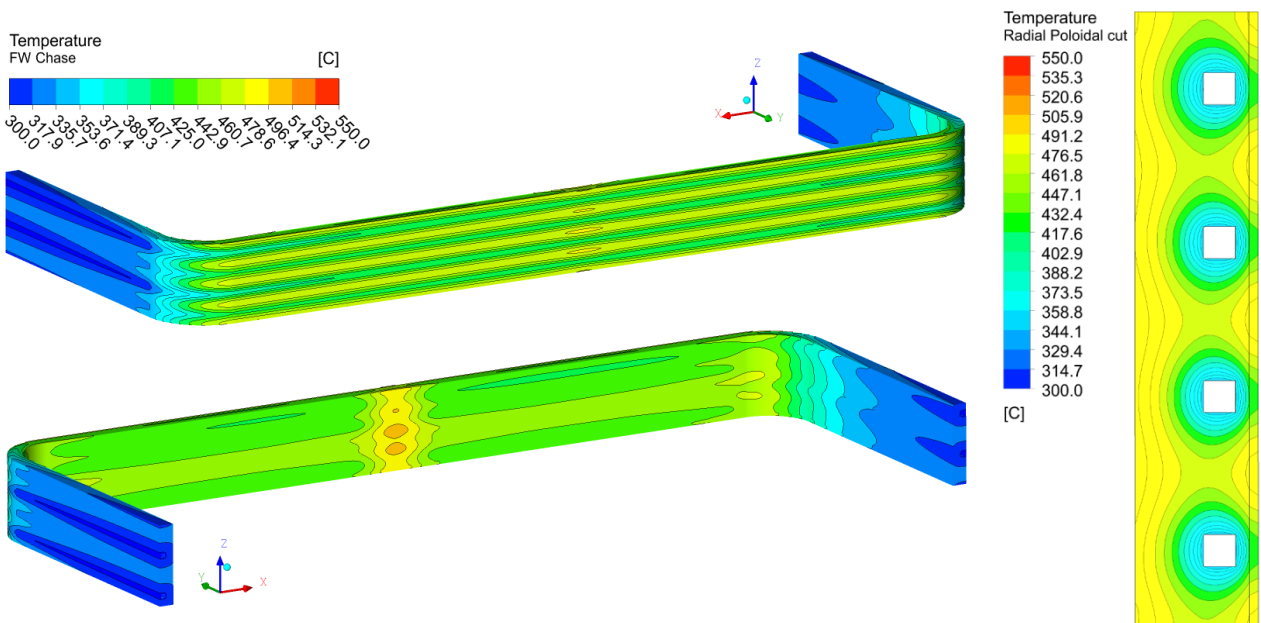
a)   FW Eurofer chase temperature field

b)   FW system radial poloidal view at half toroidal length

_____

Fig. 14: V0.6_B elementary cell FW system temperature distribution

As in the previous cases, the water mass flow rate was preliminarily evaluated to obtain the outlet conditions close to the design criteria (328°C) resulting 327.9 and 328.4, respectively for the BZ and FW cooling systems. The maximum temperature of the water reaches comparable values with the previous two cases, exceeding by about 19 degrees and 10 degrees the saturation temperature of the water at 15.5 Mpa, in the FW and BZ system respectively. Since there was no variation in the imposed mass flow rate and inlet conditions, the CHF, of BZ first tubes array and FW channel, is the same of the previous version, obtaining in the present analysis maximum heat flux values of 0.68 and 1.18 MW/m², respectively.

To evaluate the presence of PbLi hot column, that can affect the structures temperature field, different radial poloidal cuts have been evaluated (Fig. 15): one (a) in the middle of the toroidal length; the second (b) and the third (c) in correspondence of the external and internal curvature path of the first and second arrays of tubes; the fourth (d) in the middle of the toroidal path of the third tubes array; and the fifth (e) cut placed in the hot region near the sidewall.
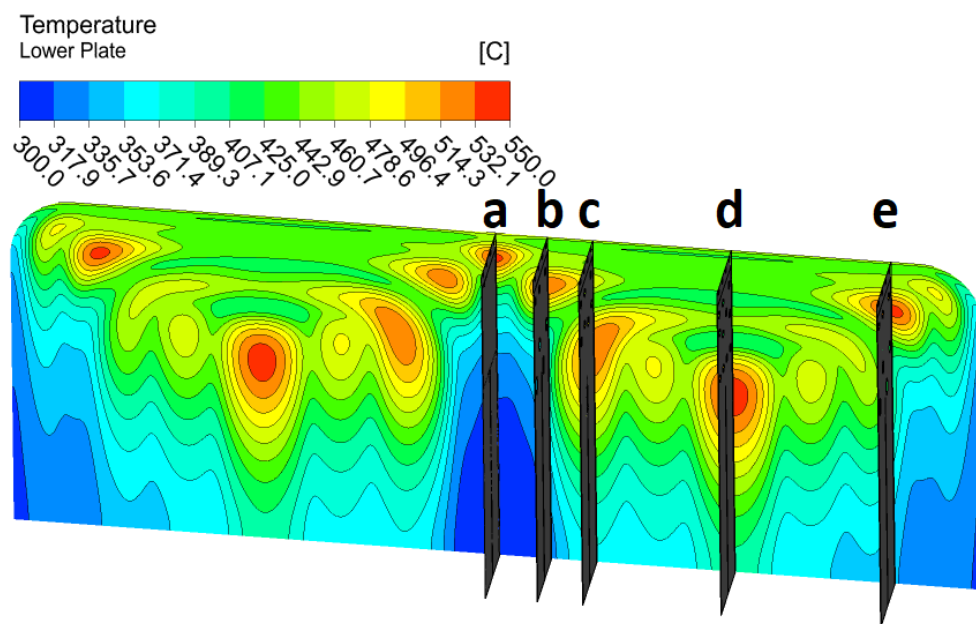

Fig. 15: V0.6_B elementary cell lower plate temperature distribution with radial poloidal cuts

The temperature distribution of each single radial poloidal cut of the V0.6_B elementary cell is reported in Fig. 16. The first cut (Fig. 16 a) shows a temperature field very similar to the V0.6_A layout. This is because it is affected only by the first tubes array with its FW detachment and curvature radius that have not been modified. The second cut (Fig. 16 b) shows a hot region, above 550°C, inside the PbLi domain, distant from the Eurofer structures and located between the first and the second tubes array. As reported in (b), the hot regions into the Eurofer plates are in the range between 513 and 532°C, ensuring a large margin from the imposed limit of 550°C. The radial poloidal cut (c) shows a hot region located at the end of the baffle plate, which poloidally extends up to both plates, but within the limit. The fourth plane (d) returns a hot region above, both in the PbLi and in the baffle plate. The listed results in Table 7 reports that the maximum temperature into the baffle plate is 552°C and Fig. 16 d shows that the region exceeding the limit (grey region) has been significantly reduced compared with the previous analyses. The last radial poloidal cut, near the sidewall, shows a hot spot region, above 550°C, within the PbLi domain. The hot spot has a grater elongation compared with the previous region and approaches, more than the others, the two plates. The plane (e) is near end of the toroidal path of the BZ water and this greatly influences the heat removal, as the water is warmer than in the previously analyzed regions. Having this area, however, Eurofer structures within the temperature limit.

_____
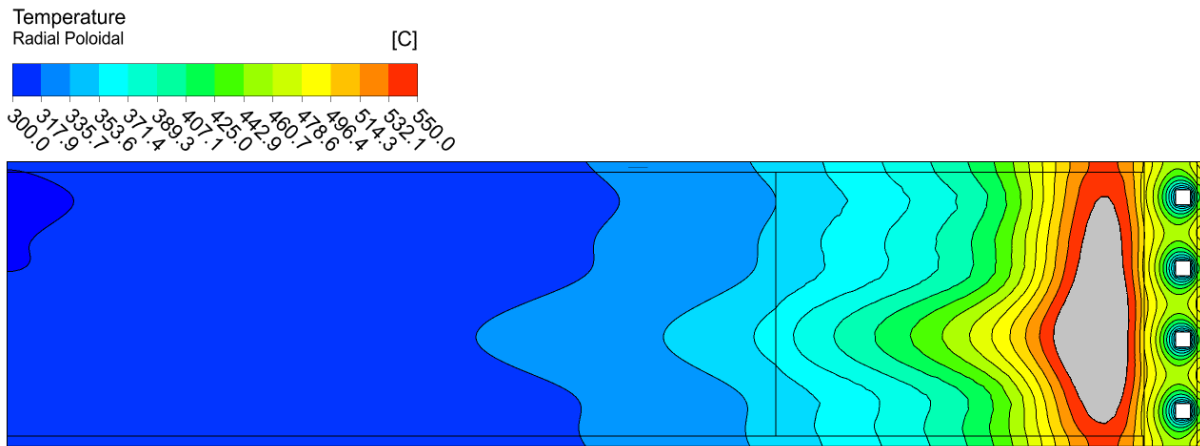
a) Central toroidal cut
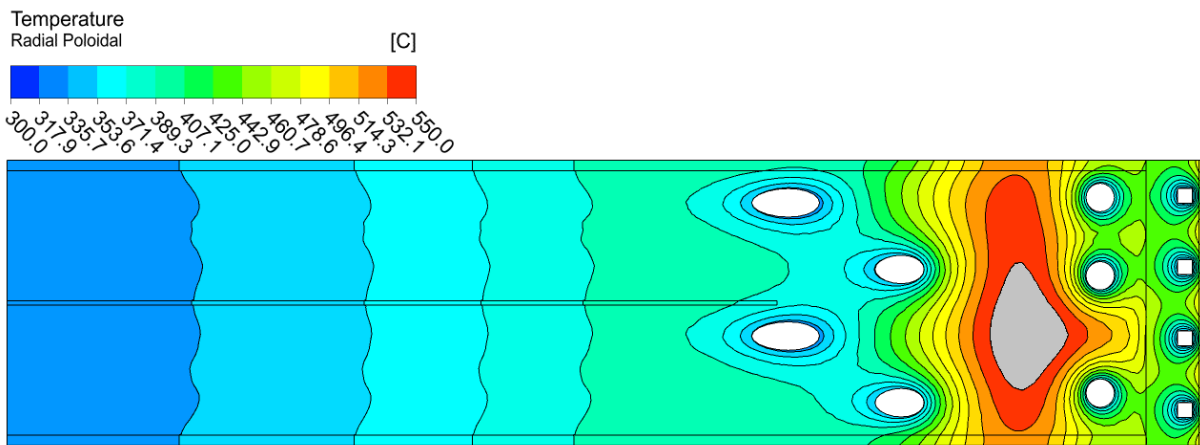
b) Second array external curvature hot region cut
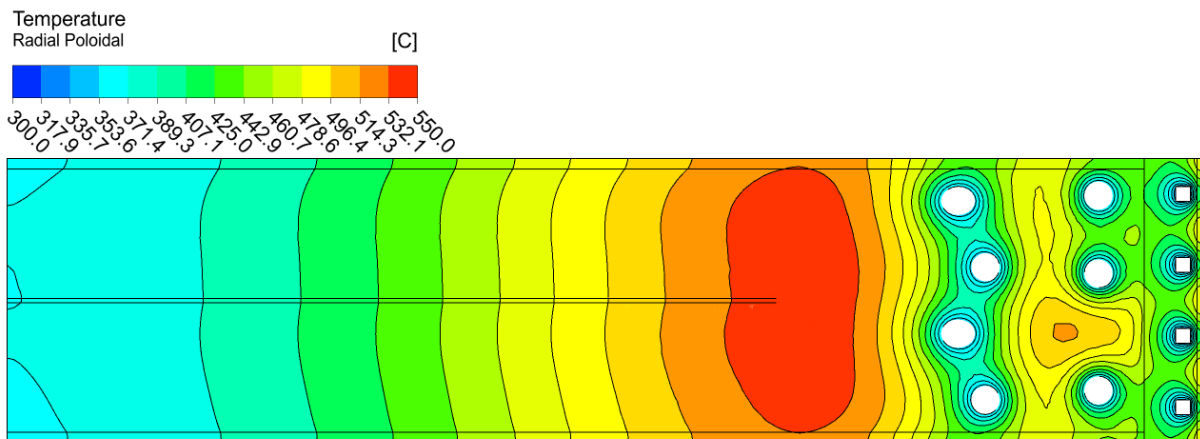
c) First and second array toroidal hot region cut

_____
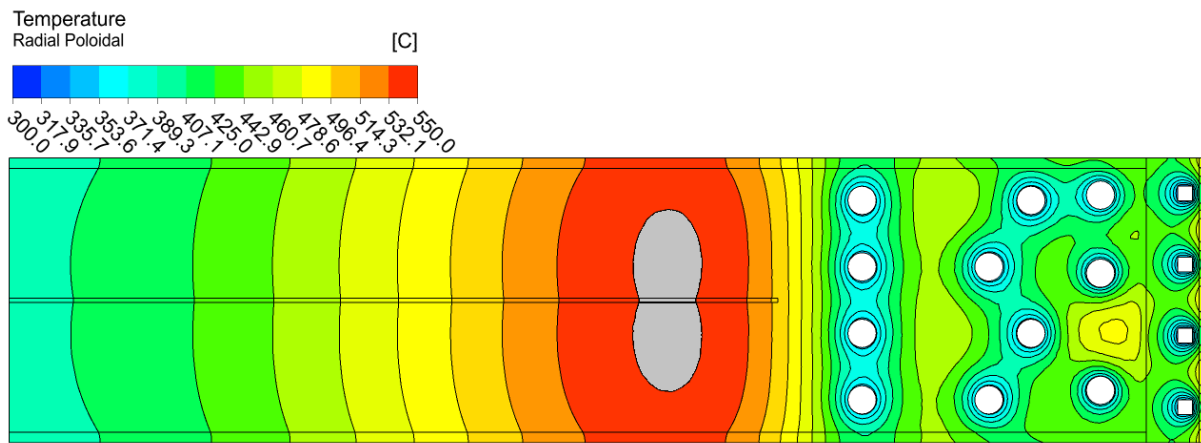
d)   Third array middle toroidal length hot region cut
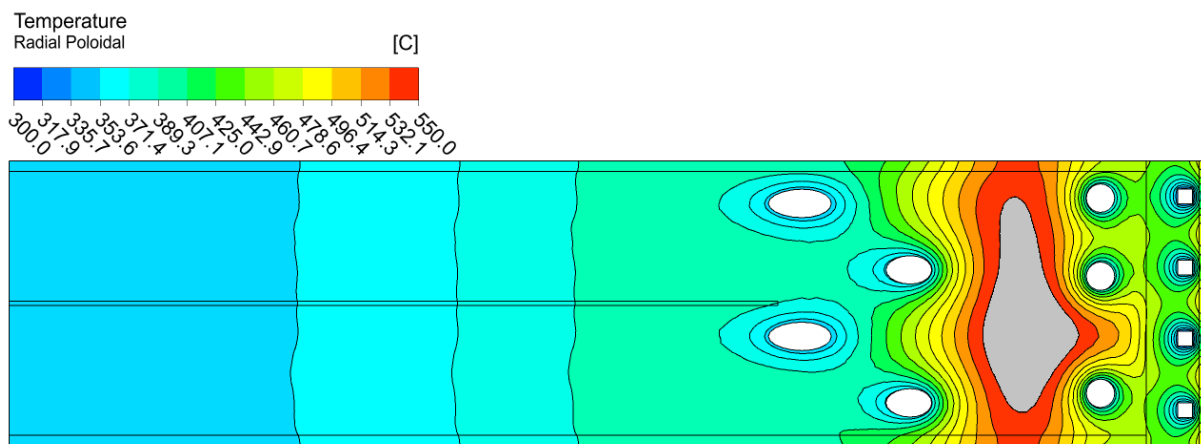
e)   Sidewall hot region cut

Fig. 16: V0.6_B different radial poloidal cuts

5. Conclusions

The cooling performance of the WCLL BB COB elementary cell has been investigated using a CFD approach, with the aim of its BZ tubes optimization. The analyses, based on the WCLL 2018 design, focused on three different BZ tubes layout of the COB equatorial elementary cell: the reference layout V0.6; the V0.6_A, with a modified tubes arrangement of the first and second tubes arrays to extinguish onset of hot spots; the V0.6_B, to further extinguish the remaining hot spots of the V0.6_A model. Computational thermal and fluid-dynamic models of these elementary cells were developed using the commercial CFD code ANSYS CFX v18.2. The heat loads adopted for the analyses are based on the most updated data, to obtain the thermal field for the most recent design. In order to optimize the BZ tubes layout, the PbLi thermal conductivity from IAEA has been adopted, because it deeply affects the structures temperature field, due to a mean percentage difference of 32% from the Mogahed recommended correlation, returning a higher temperature field compared with the latter.

The BZ recirculation ensures large safety margins to avoid the arising of thermal crisis in each model, even if subcooled nucleate boiling is expected to occur in limited regions of the BZ first tube array. Furthermore, it enhances the thermal-hydraulic performances increasing the average water velocity of the arrays. The FW water also is subjected to subcooled nucleate boiling in limited regions of the channels; moreover, it is affected by the BZ first tubes array, which affects the temperature trend inside the FW chase. The analysis has demonstrated that the BZ and FW systems are related to each other, being there heat exchange between the PbLi and FW interface. The FW cooling system must have a 13% increase of water mass flow rate to ensure adequate water conditions at the outlet compared to the effective deposited power into the system, due to the BZ and FW systems heat exchange.

The present study has demonstrated that the V0.6_B configuration can withstand the imposed heat loads and meet the DEMO design requirements, ensuring an adequate temperature field on the Eurofer upper and lower plate, FW chase and Tungsten layer, even if the baffle plate slightly exceed the temperature limit by 2 degrees. This value, however, is deemed acceptable due to the conservative criteria adopted in the present analysis and its non-structural function. Both

configurations, V0.6 and V0.6_A, are not able to keep the structural materials well below the temperature limit, exceeding 550°C in the Eurofer upper and lower plates. The reference layout V0.6 presents three different hot spots into both plates, as opposed to the V0.6_A that returns only two of them. The last configuration, the V0.6_B with its BZ tubes layout, returns a Eurofer plates temperature field without hot spots. It has been demonstrated that only the PbLi temperature rise over 550°C but with safety margins from the Eurofer structures. The V0.6_B BZ tubes layout can be considered as a promising improvement in the current design, suitable to fully withstands the steady-state thermal loads.

Further studies will be conducted with transient analysis to consider the real thermal inertia of the system and the large PbLi thermal conductivity. Moreover, analyses should be performed with transient simulation making vary the heat loads in order to evaluate the pulsed operating phase of the DEMO reactor and the response of the WCLL V0.6_B elementary cell under operating conditions that can lead to temperatures above the limit in the Eurofer structures. In addition, modelling the eventual phase change, in order to evaluate the perturbation in the system due to possible subcooled boiling and the use of different turbulence models, would be a remarkable improvement.

Acknowledgments

References

[1]   G. Federici, et al., An overview of the EU breeding blanket design strategy as an integral part of the DEMO design effort, *Fusion Engineering and Des*ign, Vol. 141, 2019, pp. 30-42. DOI: 10.1016/j.fusengdes.2019.01.141

[2]   E. Martelli, et al., Advancements in DEMO WCLL breeding blanket design and integration. *Int. J. Energy Res.*, Vol. 42, 2018, Pages 27-52. DOI:10.1002/er.3750

[3]   G. Aiello, et al., Assessment of design limits and criteria requirements for Eurofer structures in TBM components, *J. Nucl. Mater.*, 414 (2011), pp. 53-68. DOI: 10.1016/j.jnucmat.2011.05.005

[4]   D. Sornin, A. Li Puma, C. Schweier, WPBB-DEL- BB-7.1.1-T003-D001, EFDA D 2NBQ6U, Assessment of Manufacturing Technologies for Blanket Development (WCLL) / 2017 status of WCLL manufacturing activities, Eurofusion, 2018

[5]   Thermophysical Properties of Materials For Nuclear Engineering: A Tutorial and Collection of Data, IAEA, Vienna, 2008, ISBN 978–92–0–106508–7

[6]   A. Del Nevo, et al., Recent progress in developing a feasible and integrated conceptual design of the WCLL BB in EUROfusion project, *Fusion Engineering and Design*, Volume 146, Part B, 2019, Pages 1805-1809. DOI:10.1016/j.fusengdes.2019.03.040.

[7]   F. Edemetti, et al., On the impact of the heat transfer modelling approach on the prediction of EU-DEMO WCLL breeding blanket thermal performances, *Fusion Engineering and Desing*, paper under review, in: ISFNT 2019 – 14th International Symposium on Fusion Nuclear Technology.

[8]   A. Del Nevo, et al., WCLL BB design and Integration studies 2019 activities, Internal Deliverable WPBB-DEL- BB-3.2.1-T006-D001, IDM Ref. 2P5NE5 v1.0, 12 February 2020.

[9]   F. Edemetti, et al., Optimization of the First Wall cooling system for the DEMO WCLL blanket, *Fusion Engineering and Design*, DOI: 10.1016/j.fusengdes.2020.111903.

[10] A. Tassone, et al., MHD mixed convection flow in the WCLL: Heat transfer analysis and cooling system optimization. *Fusion Engineering and Design*, (2019), 146 Part A, pp. 809-813, DOI: 10.1016/j.fusengdes.2019.01.087.

[11] A. Tassone, Study on liquid metal magnetohydrodynamic flows and numerical application to a water-cooled blanket for fusion reactors, PhD thesis, Sapienza University of Rome, February 2019

[12] E. Martelli, et al., Thermo-hydraulic analysis of EU DEMO WCLL breeding blanket. *Fusion Engineering and Design*, Vol. 130, 2018, pp. 48-55. DOI: 10.1016/j.fusengdes.2018.03.030.

[13] D. Martelli, et al., Literature review of lead-lithium thermophysical properties. *Fusion Engineering and Design*, Vol. 138, 2019, pp. 183-195. DOI: 10.1016/j.fusengdes.2018.11.028.

[14] ISL Inc, RELAP5/MOD3.3 Code Manual Volume I: Code Structure, System Models, and Solution Methods, Nuclear Safety Analysis Division, July 2003

[15] E.A. Mogahed and G.L. Kulcinski, Bibliography of a Promising Tritium Breeding Material – Pb83Li17, Fusion Technology Institute, University of Wisconsin, UWFDM-994, 1995

[16] S. Noce, et al., Nuclear analysis of the Single Module Segment WCLL DEMO, *Fusion Engineering and Design*, Vol. 147, 2019. DOI:10.1016/j.fusengdes.2019.05.026.

[17] F. Maviglia, et al., Wall protection strategies for DEMO plasma transients, *Fusion Engineering and Design*, Vol. 136, Part A, 2018, pp. 410-414. DOI:10.1016/j.fusengdes.2018.02.064.

[18] F. Maviglia, et al., Overview of DEMO Technology and Scenario Design activities in Europe, *2nd Asia-Pacific Conference on Plasma Physics (AAPPS-DPP 2018)*, Kanazawa, Japan, 12.11.2018 – 17.11.2018.

F. Edemetti, et al., *Thermal-hydraulic analysis of the DEMO WCLL elementary cell: BZ tubes layout optimization*,
Fusion Engineering and Design, 2020, https://doi.org/10.1016/j.fusengdes.2020.111956

[19] A. Tassone, et al., Recent progress in the WCLL breeding blanket design for the DEMO fusion reactor, *IEEE Transactions on Plasma Science*, Vol. 46, 2018, pp. 1446-1457. DOI:10.1109/TPS.2017.2786046

[20] F. Edemetti, et al., DEMO WCLL breeding zone cooling system design: Analysis and discussion. *Fusion Engineering and Design*, Vol. 146, Part B, 2019, pp. 2632-2638. DOI: 10.1016/j.fusengdes.2019.04.063.

[21] I. Di Piazza, et al., Numerical prediction of turbulent flow and heat transfer in helically coiled pipes, *International Journal of Thermal Sciences*, Volume 49, Issue 4, 2010, pp. 653-663. DOI: 10.1016/j.ijthermalsci.2009.10.001.

[22] Ansys inc., Ansys CFX reference guide, release 18.2, USA.

[23] M. Shah, A general correlation for critical heat flux in horizontal channels, *International Journal of Refrigeration*, 2015. DOI:10.1016/j.ijrefrig.2015.06.027.

[24] L.S. Tong, A phenomenological study of critical heat flux, ASME Paper 75-HT-68, 1975.